The Meteoritical Society

Meteoritics & Planetary Science 52, Nr 9, 1763–1775 (2017)
doi: 10.1111/maps.12885

Crystal structure refinement of chromites from two achondrites, their T-$f(O_2)$ conditions, and implications

Davide LENAZ[1,*] and Birger SCHMITZ[2]

[1]Department of Mathematics and Geosciences, University of Trieste, Trieste, Italy
[2]Division of Nuclear Physics, Department of Physics, Lund University, Lund, Sweden
[*]Corresponding author. E-mail: lenaz@units.it

(Received 09 February 2016; revision accepted 23 March 2017)

Abstract–Six Cr-spinel grains from NWA 6077 brachinite-like and NWA 725 winonaite achondrites have been studied by single-crystal X-ray diffraction and structural refinement. From a chemical point of view, spinels from NWA 6077 show Cr/(Cr + Al) (i.e., Cr#) and Mg/(Mg + Fe^{2+}) (i.e., Mg#) values similar to other brachinites, while the Cr# of NWA 725 is lower than that of literature winonaites. Spinels from NWA 6077 and NWA 725 meteorites show similar cell edges, while the oxygen positional parameter is rather different being about 0.2629 for NWA 6077 and 0.2622 for NWA 725. Considering both parameters, NWA 725 shows structural features that are close to some terrestrial spinel occurrences as in komatiites, kimberlites, or included in diamonds; those from NWA 6077 show values that have no terrestrial analogs. Olivine-chromite closure temperature ranges from ~737 to ~765° C for NWA 725, being similar to that of literature winonaites and ~846 to ~884° C for NWA 6077. The logfO_2 ranges from −19.8 to −20.5 and −17.0 to −17.9 for the two meteorites, respectively. The *u* values for terrestrial samples can give information about the cooling history of the samples. For the extraterrestrial samples, it seems that it can give information about the cooling only for spinels where it is lower than 0.2625. For higher values, it appears related only to the chemistry of the spinels.

INTRODUCTION

Chromite is a common oxide accessory phase in terrestrial, Martian, and lunar mafic and ultramafic rocks. In terrestrial and Martian systems, Cr usually occurs as Cr^{3+} stabilizing Cr-spinel, whereas in more reducing environments, there could be a substantial amount of Cr^{2+} (Sutton et al. 1993), for example, delaying the crystallization of chromite from lunar melts (Schreiber and Haskin 1976; Seifert and Ringwood 1988). Chromite is usually present also in ordinary chondrites, where it has been studied since the 1960s to find relations between the Fe, Mg content of chromites to that of olivines in the H, L, and LL groups of equilibrated chondrites (Bunch et al. 1967). Moreover, chromite is an accessory phase also in nonchondritic meteorites such as winonaites, pallasites, brachinites, ureilites, diogenites, and eucrites (Mittlefehldt et al. 1998). In particular, chromites are present in most main-group pallasites with Cr#, i.e., Cr/(Cr + Al), in the range 0.84–0.97, and Mg#, i.e., Mg/(Mg + Fe^{2+}), in the range 0.24–0.36. Chromites are rare in most ureilites, and in higher-Fo ureilites, they are absent due to the formation at lower fO_2, out of the range of Cr^{3+} stability. Recently, Goodrich et al. (2014) studied several occurrences of chromite in ureilites and found that it occurs as subhedral to anhedral grains comparable in size (~30 μm to 1 mm) and/or textural setting to the major silicates in respective rock, indicating that it is a primary phase. The most FeO-rich chromites in these samples are the ones with the most primitive compositions preserved (Mg# = 0.45–0.40; Cr# varying from 0.65 to 0.72 among samples). In diogenites and eucrites, the Cr# ranges from 0.5 to 1, while Mg# is below 0.29 (Mittlefehldt et al. [1998] and references therein). According to Day et al. (2012), chromite occurs interstitially and as inclusions in brachinites showing two dominant chromite

compositions. There are low-Al chromites (Cr# = 0.82–0.84) and high Al compositions (Cr# = 0.71–0.74). Typically they have low Fe_2O_3.

Chromium-bearing spinels have been utilized extensively as a petrogenetic indicator because Cr-spinel composition is a rich source of information on the origin and evolution of parent magma composition (Irvine 1967; Dick and Bullen 1984; Lenaz et al. 2000; Barnes and Roeder 2001; Kamenetsky et al. 2001). More recently several workers studied the relationships between mineral chemistry, structural parameters (essentially cell edge a_0 and oxygen positional parameter u, i.e., the position of the oxygen along the cell diagonal), and tectonic setting (Della Giusta et al. 1986; Princivalle et al. 1989; Carbonin et al. 1999; Carraro 2003; Bosi et al. 2004; Lenaz et al. 2004a; Uchida et al. 2005).

This study presents structural and chemical data of six Cr-bearing spinels from the NWA 6077 brachinite-like and NWA 725 and winonaite achondrites. The Cr/(Cr + Al) (Cr#) and the $Mg/(Mg + Fe^{2+})$ (Mg#) of spinels from meteorites is rather different from that of terrestrial samples. We selected one winonaite achondrite because the spinels in winonaites show the highest Cr# registered for natural spinels (Bunch et al. 1970; Takeda et al. 2000; Benedix et al. 2005). Spinels from brachinites show Cr# and Mg# values (Keil 2014) that are rather close to some terrestrial occurrences for which X-ray single-crystal data are available (Lenaz et al. 2004a, 2007, 2009, 2012). Moreover, their chemistry is rather similar to that of some spinels from chondrite already studied by Lenaz et al. (2015). Here, we compile the first integrated crystal-chemical data set of natural Cr-spinels in these meteorites and discuss them in comparison with previously analyzed chondrite spinels (Lenaz et al. 2015) and terrestrial analogs in order to verify if the cooling history of spinels, as supposed by the structural parameter u, can be determined for extraterrestrial spinels and be used coupled with estimated closure temperatures. Moreover, oxygen fugacities will be calculated for these two meteorites and compared with meteorite analogs.

MATERIALS AND BACKGROUND

According to Garvie (2012), NWA 6077 is classified as an achondrite meteorite (ungrouped, brachinite-like) with an olivine-rich ($Fa_{30.2\text{-}30.7}$) assemblage with protogranular (possibly cumulate) texture exhibiting triple-junction grain boundaries. Additional minerals include orthopyroxene ($Fs_{24.1\text{-}24.5}Wo_{2.1\text{-}2.0}$), clinopyroxene ($Wo_{44.0\text{-}43.5}Fs_{9.4\text{-}10.0}$), altered kamacite, chromite, chlorapatite, Ni-bearing troilite, and/or pyrrhotite. Brachinites and brachinite-like achondrites can broadly be defined as olivine-rich rocks (modal olivine 68–95%) that, using a terrestrial terminology, can be described as wehrlites and dunites. They contain Ca-rich pyroxene and accessory phases of plagioclase, orthopyroxene, chromite, sulfide, metal, and phosphates. NWA 6077 experienced some minor terrestrial weathering, resulting in partial alteration of primary metals, as well as veining within fractures by calcite, clay minerals, and iron hydroxides. It is considered a brachinite-like meteorite because it shares similarities with brachinites but probably originated from a different parent body. New isotopic data by Sanborn et al. (2016) show how the $\varepsilon^{53}Cr$ equal to 0.21 ± 0.04 of chromite fractions distinguishes this meteorite from the typical brachinite. Recent work determining the isotopic composition for O, Ca, Ti, Ni, Mo, and Ru showed that there are similarities in O and Ni between NWA 5400, the paired sample NWA 5363, and Earth, while Ca, Ti, Mo, and Ru are resolvable from Earth so that the true composition of the source reservoir of NWA 5400 is still an open question.

The NWA 725 meteorite is, according to Grossman and Zipfel (2001), an acapulcoite with olivine ($Fa_{6.1}$), orthopyroxene ($Wo_0Fs_{7.5}$), and clinopyroxene ($Wo_{46}En_{50.9}$ $Fs_{3.1}$), but Greenwood et al. (2012) on the basis of its oxygen isotope composition ascribed it to winonaites. According to Benedix et al. (1998), winonaites have mineral compositions, mineralogy, and oxygen isotopic compositions distinct from primitive achondrite groups other than silicate inclusions in IAB and IIICD irons but lacking the metallic matrices of the latter and consist mostly of silicates. These authors suggested that winonaites formed from a chondritic precursor material with different mineral and oxygen isotopic compositions with respect to known chondrites. Extensive heating caused metamorphism and partial melting of both Fe,Ni-FeS and silicate material. Recrystallization followed impact brecciation with consequent cooling that mixed lithologies with different thermal histories and metamorphism.

METHODS

The meteorites are cut to an appropriate size, typically 1–4 g, and treated in an ultrasonic bath, washed, and dried. The cleaned meteorites are placed in an HF-resistant plastic net sitting in a 1-liter plastic beaker so that the bottom of the net is approximately 2 cm above the bottom of the beaker. One part of water and three parts of HF (40%) are poured into the beaker, and after 3–7 days, the meteorites are completely disintegrated and appear as a dark sediment layer at the bottom of the beaker. The sample is pH-neutralized by means of water decanting and then sieved through a 32-μm sieve. The residual material is divided into two size fractions: >63 μm and 32–63 μm,

respectively. After drying, the sample is submerged in 95% ethanol and representative spinel grains are picked under a light microscope.

X-ray diffraction data for the six chromite grains analyzed were recorded on an automated KUMA-KM4 (K-geometry) diffractometer, using MoKα radiation, monochromatized by a flat graphite crystal. Twenty-four equivalent reflections of the (12 8 4) peak, at about 80° 2θ, were accurately centered at both sides of 2θ, and the α_1 peak barycenter was used for cell parameter determination. Data collection was made, according to Della Giusta et al. (1996), up to 50° θ in the ω-2θ scan mode, scan width 1.8° 2θ, counting time from 20 to 50 s depending on the peak standard deviation. Corrections for absorption and background were performed according to North et al. (1968). Structural refinement using the SHELX-97 program (Sheldrick 2008) was carried out against Fo^2_{hkl} in the Fd-3-m space group (with origin at −3 m), since no evidence of different symmetry appeared. Scattering factors were taken from Prince (2004) and Tokonami (1965). Neutral scattering curves, Mg versus Fe in the T site, and Cr versus Al in the M site were assigned, with the constraints of full site occupancy and equal displacement parameters. Oxygen ionization varies among different grains in order to reach the best fit between structural refinement and chemical analyses and to obtain the best value for all conventional agreement factors. Results are in Table 1.

After X-ray data collection, the same crystals used for X-ray data collection were mounted on glass slides, polished, and carbon coated for electron microprobe analyses on a CAMECA-SX50 microprobe at IGG-CNR, Padua, operating at 15 kV and 15 nA. A 20-s counting time was used for both peak and total background. Synthetic $MgCr_2O_4$ and $FeCr_2O_4$ spinels (Lenaz et al. 2004b) have been used for Mg, Cr, and Fe determination; Al_2O_3 for Al; $MnTiO_3$ for Ti, Mn; NiO for Ni; and sphalerite for Zn. Up to 15 spot analyses were performed on each crystal to verify zoning and possible nonhomogeneity in composition. Raw data were reduced by PAP-type correction software provided by CAMECA. Results are in Table 1.

Several different procedures may be adopted to determine cation distribution, and very satisfactory results have recently been obtained by combining data from single-crystal X-ray structural refinements and electron microprobe analyses. This procedure simultaneously takes into account both structural and chemical data and reproduces the observed parameters by optimizing cation distributions. Differences between measured and calculated parameters are minimized by a function $F(X)$ taking in consideration different parameters as the observed quantity and their standard deviations, cation fractions in T and M sites, unit cell and oxygen parameter, mean atomic number of T and M sites, atomic proportions given by microprobe analyses, and constraints imposed by crystal chemistry (total charges and occupancies of T and M sites). The cation distribution for the present samples has been achieved by using the Carbonin et al. (1996) and Lavina et al. (2002) model, later summarized in Lenaz et al. (2015). This model yields cation distribution by minimizing the weighted differences between observed crystal-chemical data and data calculated from site atomic fractions. This cation distribution in the tetrahedral (T) and octahedral (M) sites must be consistent with the assumptions that the mean atomic number (m.a.n.) corresponds to:

$$\text{m.a.n.T} = \sum_i {}^{\text{IV}}X_i N_i \quad (1)$$

$$\text{m.a.n.M} = \sum_i {}^{\text{IV}}X_i N_i \quad (2)$$

where ${}^{\text{IV}}X_i$ and ${}^{\text{VI}}X_i$ are chemical species in T and M, respectively, and N is their atomic number. The site bond length arises from a linear contribution of each species to the tetrahedral (T-O) and octahedral (M-O) coordination distances so that:

$$\text{T} - \text{O} = \sum_i {}^{\text{IV}}X_i {}^{\text{IV}}D_i \quad (3)$$

$$\text{M} - \text{O} = \sum_i {}^{\text{VI}}X_i {}^{\text{VI}}D_i \quad (4)$$

where ${}^{\text{IV}}D_i$ and ${}^{\text{VI}}D_i$ are the cation-to-oxygen bond distances of each cation in tetrahedral and octahedral coordination, respectively.

Summarizing, site atomic fractions ${}^{\text{IV}}X_i$ and ${}^{\text{VI}}X_i$ must satisfy the above equations but must also total the atomic proportions from chemical analyses and obey three crystal-chemical constraints: occupancies of T and M sites and formal valence so that ${}^{\text{IV}}X_i$ and ${}^{\text{VI}}X_i$ may be calculated by minimizing the following sum of residuals:

$$F(X_i) = \frac{1}{n}\sum\nolimits_{j=1}^{n}\left(\frac{Oj - Cj(X_i)}{\sigma j}\right)^2 \quad (5)$$

where O_j are the observed quantities with their standard deviation σ_j. O_j are the four observed crystallographic parameters (a, u, and m.a.n. of T and M sites) and the chemical proportions for a total of n. $C_j(X_i)$ are the corresponding quantities calculated by means of variable cation fractions X_i. Results are shown in Table 1.

Table 1. Results of crystal structure refinements, chemical analyses, cation distribution, olivine-chromite closure temperature, and oxygen fugacities of studied chromite.

Sample	NWA725A	NWA725B	NWA725C	NWA6077A	NWA6077B	NWA6077C
a	8.3386 (1)	8.3362 (1)	8.3433 (4)	8.3340 (2)	8.3331 (2)	8.3352 (1)
u	0.2622 (1)	0.2622 (1)	0.2623 (1)	0.2630 (1)	0.26292 (9)	0.26290 (9)
m.a.n.T	18.9 (3)	18.9 (3)	19.6 (4)	22.2 (8)	23.1 (3)	22.8 (6)
m.a.n.M	22.7 (5)	22.6 (5)	23.2 (7)	20.8 (1.1)	22.0 (3)	21.4 (8)
U (M)	0.0039 (1)	0.0047 (1)	0.0043 (1)	0.0036 (3)	0.0042 (1)	0.0037 (2)
U (T)	0.0062 (2)	0.0066 (2)	0.0063 (3)	0.0068 (3)	0.0072 (2)	0.0069 (2)
U (O)	0.0056 (2)	0.0066 (3)	0.0058 (3)	0.0069 (4)	0.0060 (2)	0.0064 (4)
N. refl.	168	139	139	151	155	150
R1	2.43	2.08	2.17	2.88	2.26	2.12
wR2	5.12	4.42	4.92	6.11	4.91	4.99
GooF	1.245	1.086	1.190	1.173	1.317	1.186
MgO	9.9 (1)	9.7 (1)	9.69 (9)	4.4 (2)	4.7 (1)	4.57 (5)
Al_2O_3	4.9 (2)	5.8 (2)	5.5 (2)	8.16 (4)	8.12 (7)	8.25 (9)
TiO_2	1.02 (4)	0.84 (4)	1.01 (3)	1.44 (4)	1.47 (3)	1.44 (4)
Cr_2O_3	65.9 (4)	65.0 (3)	65.3 (5)	57.6 (5)	57.8 (4)	57.6 (3)
MnO	1.91 (6)	2.2 (2)	2.3 (2)	0.44 (4)	0.43 (5)	0.47 (3)
FeO	16.5 (2)	16.7 (3)	16.9 (2)	27.8 (4)	27.6 (2)	27.6 (3)
NiO*	0.01 (1)	0.00 (1)	0.01 (1)	0.01 (1)	0.01 (2)	0.01 (2)
ZnO*	0.01 (2)	0.01 (1)	0.01 (2)	0.16 (9)	0.15 (5)	0.12 (8)
Sum	100.2	100.2	100.6	100.1	100.3	100.1
T Site						
Mg	0.461 (5)	0.489 (5)	0.452 (5)	0.222 (8)	0.214 (5)	0.237 (3)
Al	0.026 (3)	0.019 (2)	0.015 (2)	0.0020 (2)	0.0102 (5)	0.0070 (5)
Mn	0.055 (2)	0.060 (6)	0.065 (5)	0.013 (1)	0.012 (2)	0.0140 (9)
Fe^{2+}	0.459 (5)	0.432 (6)	0.468 (6)	0.763 (9)	0.753 (6)	0.727 (7)
Fe^{3+}				0.0000 (1)	0.006 (3)	0.015 (4)
Zn					0.004 (1)	
M Site						
Mg	0.039 (2)	0.0007 (2)	0.034 (1)	0.007 (2)	0.028 (2)	0.0004 (1)
Al	0.169 (7)	0.221 (8)	0.200 (9)	0.333 (3)	0.321 (3)	0.330 (4)
Ti	0.026 (1)	0.021 (1)	0.0255 (8)	0.038 (1)	0.0384 (8)	0.027 (1)
Cr	1.756 (8)	1.720 (9)	1.733 (6)	1.582 (9)	1.578 (7)	1.584 (7)
Fe^{2+}	0.0095 (7)	0.038 (2)	0.0084 (7)	0.027 (2)	0.0215 (9)	0.046 (2)
Fe^{3+}				0.012 (9)	0.012 (5)	0.011 (4)
Cr#	0.90	0.88	0.89	0.82	0.83	0.82
Mg#	0.52	0.51	0.51	0.23	0.24	0.24
F(X)	0.190	0.235	0.063	0.336	0.361	0.288
Ol-Sp Therm	765.1	736.8	741.7	845.6	883.8	863.8
fO_2	−19.80	−20.55	−20.41	−17.87	−17.05	−17.47

*Ni and, occasionally, Zn not present in cation distribution because of the deviation higher than 2σ.

a: cell parameter (Å); *u*: oxygen positional parameter; m.a.n.T and M: mean atomic number; U(M), U(T), U(O): displacement parameters for M site, T site, and O; N. Refl.: number of unique reflections (Sheldrick 2008); R1 all (%): residual index for all reflections (Sheldrick 2008); wR2 (%): weighted residual index for reflections with $I > 4\sigma$ (Sheldrick 2008); GooF: goodness of fit (Sheldrick 2008). Space Group: Fd-3 m. Origin fixed at –3 m. Z = 8. Reciprocal space range: $-19 \le h \le 19$; $0 \le k \le 19$; $0 \le l \le 19$. *F*(x): minimization factor, which takes into account the mean of square differences between calculated and observed parameters, divided by their standard deviations. Ol-sp Therm: olivine-spinel closure temperature (Ballhaus et al. 1991); fO_2: oxygen fugacity (O'Neill 1987). Estimated standard deviations are in brackets.

RESULTS AND DISCUSSION

In spinel, the anions form a nearly cubic close-packed array, stacked parallel to the (111) planes, and the cations fill a part of the tetrahedral (T) and octahedral (M) interstices available in the framework (Fig. 1). The oxygen atom is linked to three octahedral cations and one tetrahedral cation lying on opposite sides of the oxygen layer, respectively, to form a trigonal pyramid. Displacement of the oxygen atom along the cube diagonal [111] causes the oxygen layers in the spinel structure to be slightly puckered. In this way, variations in the oxygen positional parameter, so-called *u*, correspond to displacements of the oxygen

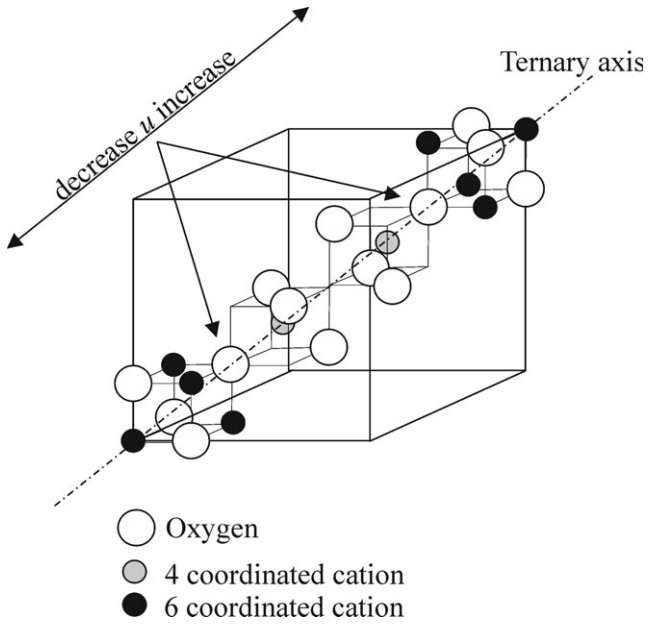

Fig. 1. Spinel structure (modified after Lindsley 1976).

atoms along the cube diagonal, and reflect adjustments to the relative effective radii of cations in the tetrahedral and octahedral sites. An increase in *u* corresponds to a relative enlargement of the tetrahedral coordination polyhedra and a compensating decrease in the octahedra (Lindsley 1976) (Fig. 1). Many studies that integrate measurements of crystal structural parameters and mineral chemical analyses have been previously performed on Cr-spinels from mantle nodules (Della Giusta et al. 1986; Princivalle et al. 1989, 2014; Carraro 2003; Uchida et al. 2005; Nédli et al. 2008; Lenaz et al. 2014c, 2017), ophiolites (Bosi et al. 2004; Derbyshire et al. 2013; Lenaz et al. 2014a, 2014b), Alpine peridotites (Lenaz et al. 2010, 2016), layered mafic intrusions (e.g., Bushveld, Rum, and Stillwater Complexes; Lenaz et al. 2007, 2011, 2012), kimberlites and spinels included in diamonds (Lenaz et al. 2009), komatiites (Lenaz et al. 2004a), and oxidized occurrences in sedimentary environments (Carbonin et al. 1999; Lenaz et al. 2002) to better understand Cr-spinel petrogenesis, oxidation mechanisms, and cooling rates. The only study taking into account the structural parameters of chromite from the extraterrestrial environment is by Lenaz et al. (2015). There the authors studied some chromites from H-chondrites and an acapulcoite and from a fossil Österplana L6 chondrite.

From a structural point of view, Cr-spinels from both NWA 725 and NWA 6077 have very similar cell edges ranging from 8.3331 (2) to 8.3433 (4) Å, while the oxygen positional parameter is quite different, being 0.2622 (1) to 0.2623 (1) for NWA 725 spinels and 0.2629 (1) to 0.2630 (1) for NWA 6077 (Table 1; Fig. 2). Lenaz et al. (2015) found that spinels from H6 meteorites present a longer cell edge (8.3480–8.3501 Å), while the others show values similar to those of the spinels studied here. The oxygen positional parameter is between 0.2624 and 0.2630.

The spinels of NWA 725 are richer in Cr_2O_3, MgO, and MnO with respect to those of NWA 6077. In both cases, Cr_2O_3 is the most abundant oxide (about 65 wt% and about 57 wt%, respectively), followed by FeO (about 17% versus 28%). Then, in NWA 725, there follows MgO (~10%), Al_2O_3 (~5%), MnO (~2%), and TiO_2 (~1%). The NWA 6077 spinels also contain Al_2O_3 (~8%), MgO (~4%), TiO_2 (~1.5%), MnO (~0.4%), and ZnO (~0.15%) (Table 1). According to stoichiometry, trivalent iron has been found only in NWA 6077 spinels in very low amounts (0.4–1.01 wt%) (Table 1). According to our chemical analyses, it appears that there is no zoning and that differences in chemical compositions of the spinels within the meteorite are very small.

According to O'Neill and Navrotsky (1984), the large excess octahedral crystal field stabilization energy of Cr^{3+} (Δ $CFSE_{(oct\text{-}tet)}$ is about 160 kJ mol^{-1}) should ensure that Cr solely enters the M site. This means that, in the studied cases, ~87% and ~80% of the octahedral sites occupied by cations of spinels in NWA 725 and NWA 6077, respectively, are filled by Cr. Even titanium can be assumed to occupy solely this site, so that only a minor amount of other elements could enter this site. In the studied spinels, these cations are Al and Fe^{3+}, with only a minor amount of divalent cations present in M. Consequently, cation assignment, taking in account structural and chemical parameters, shows an ordered distribution (Table 1).

Primitive achondrites are generally considered to represent meteorites that have experienced high-grade metamorphism, which in some cases resulted in partial melting. They fill the gap between chondrites and differentiated achondrites and represent mantle material derived from asteroids with metal cores (Benedix et al. 1998; Weisberg et al. 2006; Floss et al. 2008; Touboul et al. 2009). Primitive achondrites can retain compositional, isotopic, and textural features of their precursor materials (McCoy et al. 2006) while, texturally, ranging from metamorphosed- and anatectic-chondritic materials, such as winonaites (Benedix et al. 1998) and acapulcoites (e.g., Mittlefehldt et al. 1996), to lithologies that suffered partial melting, melt extraction, or are themselves partial melt products, such as lodranites (e.g., Mittlefehldt et al. 1996; McCoy et al. 1997), ureilites (e.g., Warren et al. 2006; Goodrich et al. 2007), brachinites (e.g., Mittlefehldt et al. 2003), and silicate inclusions within IAB and IIICD iron meteorites (e.g., McCoy et al. 1993; Choi et al. 1995). When considering the chemistry of the most abundant oxides by using the

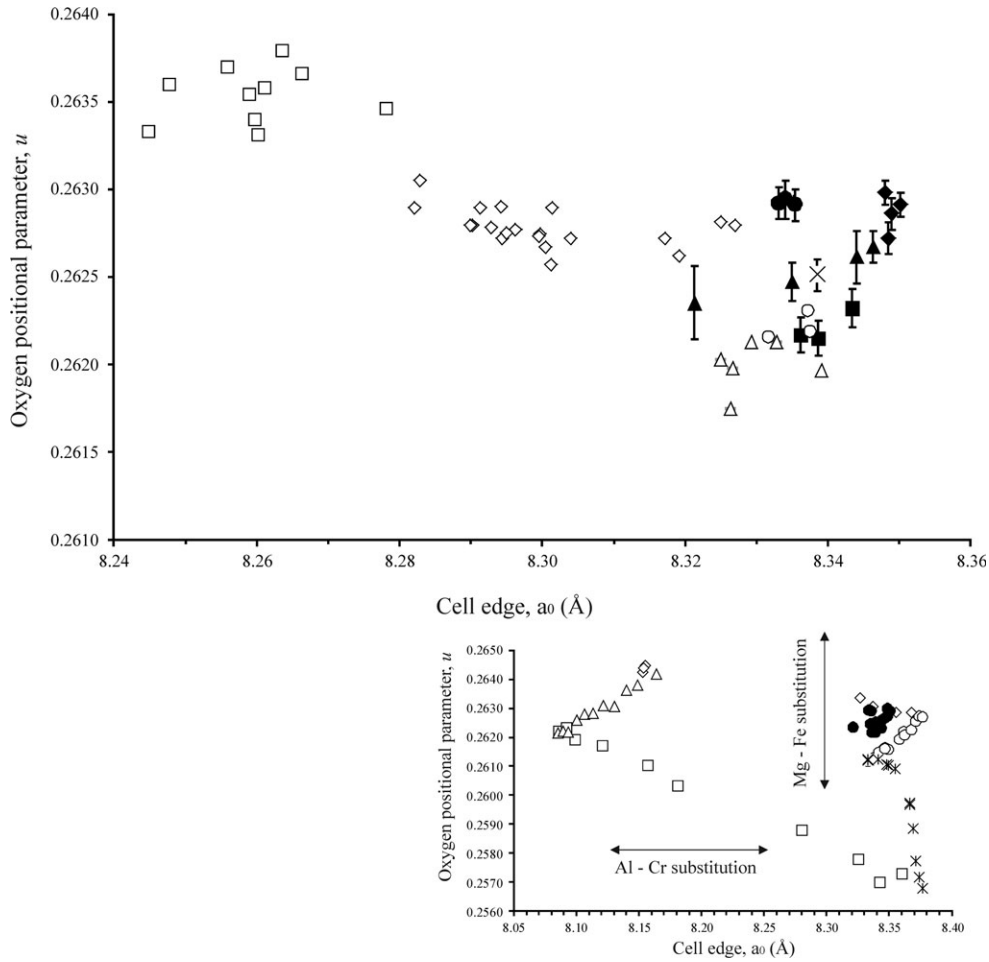

Fig. 2. Oxygen positional parameter, *u* versus cell edge, a. Black circle: NWA 6077; black square: NWA 725; black diamond: H6 chondrite (Lenaz et al. 2015); black X: acapulcoite (Lenaz et al. 2015); black triangle: detrital meteoritic spinels (GOL spinels in Lenaz et al. 2015); open triangle: chromite in kimberlites and included in diamonds (Lenaz et al. 2009); open circle: chromites in komatiites (Lenaz et al. 2004a); open diamond: chromites in layered intrusions (Lenaz et al. 2007); open square: Archean occurrences (Rollinson et al. 2017; Lenaz, unpublished data). In the inset, the oxygen positional parameter, *u* versus cell edge, for synthetic series. Open triangle: $MgAl_2O_4$-$FeAl_2O_4$ (Andreozzi and Lucchesi 2002); open diamond: $FeAl_2O_4$-$FeCr_2O_4$ (Lenaz and Skogby 2013); open circle: $MgCr_2O_4$-$FeCr_2O_4$ spinels (Lenaz et al. 2004b); asterisks: $MgCr_2O_4$-$MgFe_2O_4$ spinels (Lenaz et al. 2006); open square: $MgAl_2O_4$-$MgFe_2O_4$ spinels (Nakatsuka et al. 2004); black circle: extraterrestrial occurrences (this study and Lenaz et al. 2015).

Cr# versus Mg# diagram, terrestrial and extraterrestrial Cr-spinels show a distinct behavior, the extraterrestrial ones being usually enriched in Cr and Fe with respect to the terrestrial, apart from very few occurrences. In such a context, it is interesting to notice how NWA 725 spinels fall in the same field as spinels included in diamonds, kimberlites, and komatiites, i.e., spinels originating from great depths in the mantle. The NWA 725 spinels differ from spinels in other winonaites (Bunch et al. 1970; Takeda et al. 2000; Benedix et al. 2005) (Fig. 3). The field of brachinites shows different values with Cr# ranging between 0.72 and 0.86 and Mg# in the range 0.18–0.33. In particular, NWA 6077 spinels show Cr# values similar to those of ALH 84025 and Brachina (Keil 2014), while EET99402, Hughes026, NWA 1500, NWA 3151, and NWA 4969 spinels have lower Cr# values. Chondritic spinels analyzed by Lenaz et al. (2015) show a Cr# between 0.85 and 0.87 and Mg# in the range 0.11–0.24, so that they differ slightly from the field of brachinites.

It is interesting to note that NWA 725 and NWA 6077 spinels show similar cell edges but rather different *u* values (Fig. 2). According to Lenaz et al. (2010, 2011, 2012) the cell edge is usually related to the Cr# or to the $Cr + Fe^{3+}$ content, as can be seen in Fig. 4. Small differences in the cell edge, as suggested by Lenaz et al. (2015), are possibly due to exchange of Cr for Al and Mg for Fe^{2+} (inset in Fig. 2). The oxygen positional parameter is a consequence of the cations allocated in the different T and M sites and, according to some authors (Della Giusta et al. 1986; Princivalle et al. 1989), this can reflect the cooling history of the crystal. In fact, a rapid cooling history creates disorder with

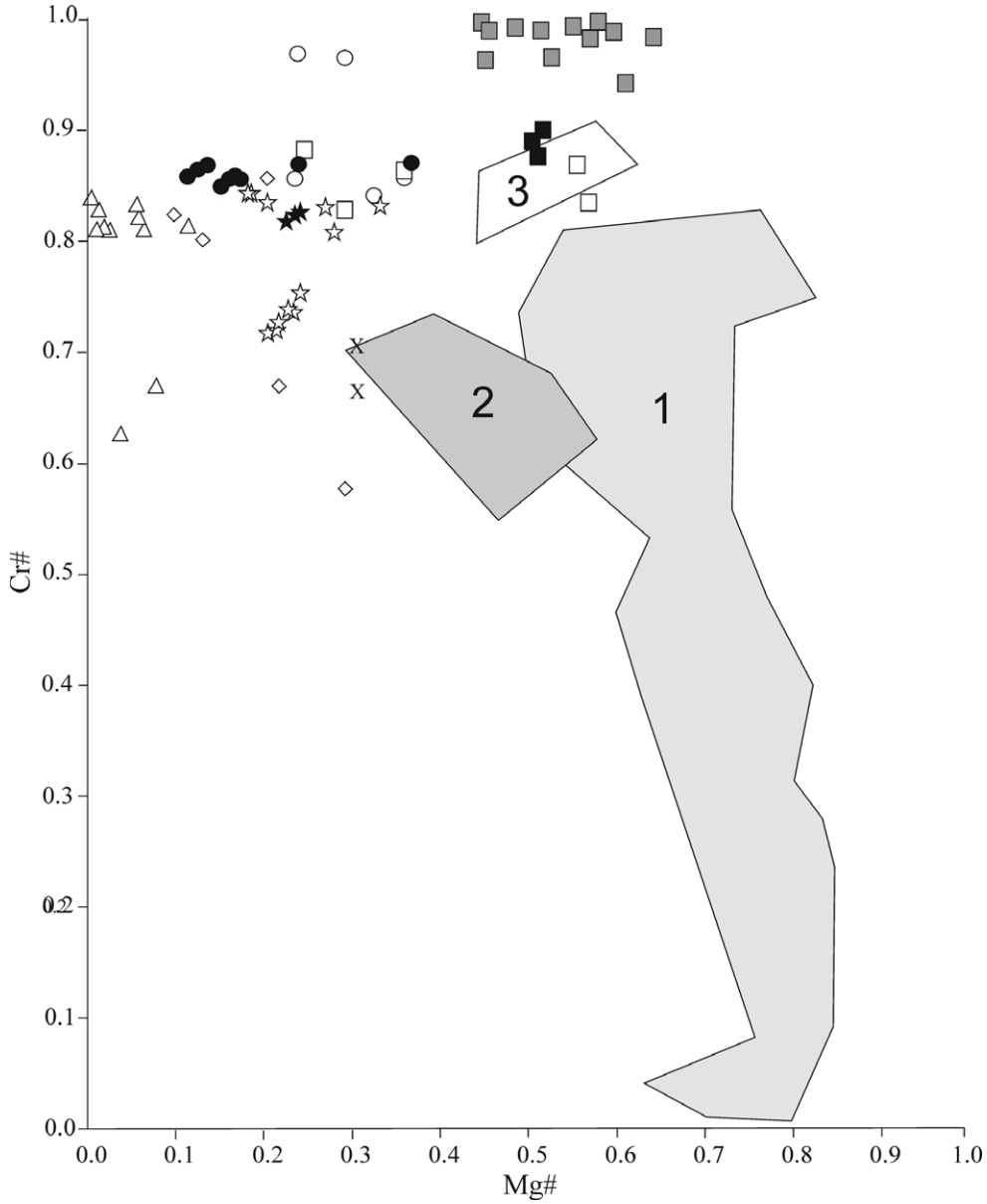

Fig. 3. Cr# (Cr/[Cr + Al]) versus Mg# (Mg/[Mg + Fe^{2+}]) diagram. Black star: NWA 6077 (this study); black square: NWA 725 (this study); open star: brachinites (Keil 2014); open circle: pallasites (Bunch and Keil 1971); open diamond: diogenites (Mittlefehldt 1994); open triangle: eucrites (Bunch and Keil 1971; Lovering 1975; Christophe Michel-Levy et al. 1987; Mittlefehldt and Lindstrom 1993; Yamaguchi et al. 1994; Buchanan and Reid 1996); gray square: winonaites (Bunch et al. 1970; Takeda et al. 2000; Benedix et al. 2005); open square: acapulcoites and lodranites (Mittlefehldt et al. 1996); black circle: H and L chondrites (Lenaz et al. 2015). Fields are for terrestrial occurrences. Field 1: mantle xenoliths, ophiolites, and Alpine peridotites (Basso et al. 1984; Della Giusta et al. 1986; Princivalle et al. 1989, 2014; Carraro 2003; Bosi et al. 2004; Uchida et al. 2005; Lenaz et al. 2010, 2014a, 2014b, 2014c, 2016, 2017; Derbyshire et al. 2013; Perinelli et al. 2014); Field 2: layered complexes (Lenaz et al. 2007, 2012); Field 3: spinels included in diamonds, kimberlites, and komatiites (Lenaz et al. 2004a, 2009, 2013). For the terrestrial fields, we used only Cr-spinels for whom structural studies are also available.

trivalent cations such as Al and/or Fe^{3+} (Parisi et al. [2014] among others) in the T site, while divalent cations Mg and Fe^{2+} in the M site. A slow cooling rate should establish an ordered situation with trivalent cations in M site and divalent in T site. This fact has been very useful in the study of spinels from mantle xenoliths where the Cr content is limited, and there is a large possibility of exchanges between Mg and Al (Princivalle et al. 1989, 2014; Carraro 2003; Nédli et al. 2008; Lenaz et al. 2014c). Contrary to many other winonaites, the piece of NWA 725 from which our analyzed spinels originate shows a clear chondrule

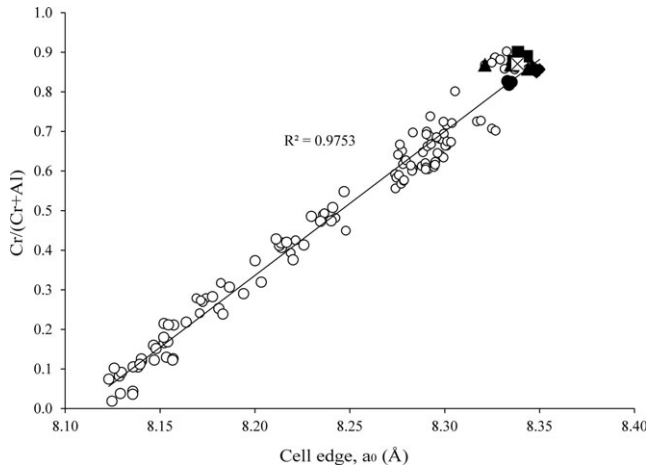

Fig. 4. Cr/(Cr + Al), versus cell edge, a_0. Extraterrestrial occurrences are represented in black symbols as in Fig. 3. Open circle: terrestrial occurrences (Della Giusta et al. 1986; Princivalle et al. 1989; Carraro 2003; Lenaz et al. 2004a, 2007, 2009, 2010, 2012; Uchida et al. 2005).

structure. This may be independent evidence that NWA 725 retains signatures of a slow cooling at significant depths in the parent body.

But what happens when there is a higher Cr content? Is it still possible to think about a distribution of Mg-Al related to the cooling history or is there a chemical control on the oxygen positional parameter? In Fig. 5, we compare the behavior of Cr/(Cr + Al), Mg/(Mg + Fe^{2+}), and Fe^{3+}/(Fe^{3+} + Al + Cr) versus the oxygen positional parameter.

By comparing Cr/(Cr + Al) versus *u*, it is possible to recognize three different behaviors. The first is represented by terrestrial and extraterrestrial spinels with very high Cr#. They display an almost flat pattern with limited Cr# variations and a large span of *u* values. The second is represented by an inverse "trend" of terrestrial spinels where large variations of Cr# and *u* values are present. The third one shows the behavior of mantle xenolith spinels and is represented by a cloud distribution of both Cr# and *u*.

When considering Mg/(Mg + Fe^{2+}) versus *u*, there are no trends shown by spinels from mantle xenoliths and other terrestrial sources. For extraterrestrial spinels, there are two different situations. Spinels with *u* values smaller than 0.2625 show a large variation of Mg# values (0.1–0.5), while those with *u* longer than 0.2625 have a more limited Mg# variation (0.1–0.25). As regards the Fe^{3+}/(Fe^{3+} + Al + Cr) versus *u*, it is not possible to find out trends; anyway, only few extraterrestrial spinels show the presence of Fe^{3+}.

These circumstances indicate that for spinels from mantle xenoliths, there is no relation between Cr# and Mg# versus the oxygen positional parameter so that the last values are effectively governed by the cooling history of the host rock. For the other terrestrial occurrences, it seems that there could be a chemical control on the *u* parameter by Cr#. For extraterrestrial spinels, there are two possibilities. For spinels with Cr# in the range 0.81–0.87 and Mg# 0.1–0.20, displacement of cations among

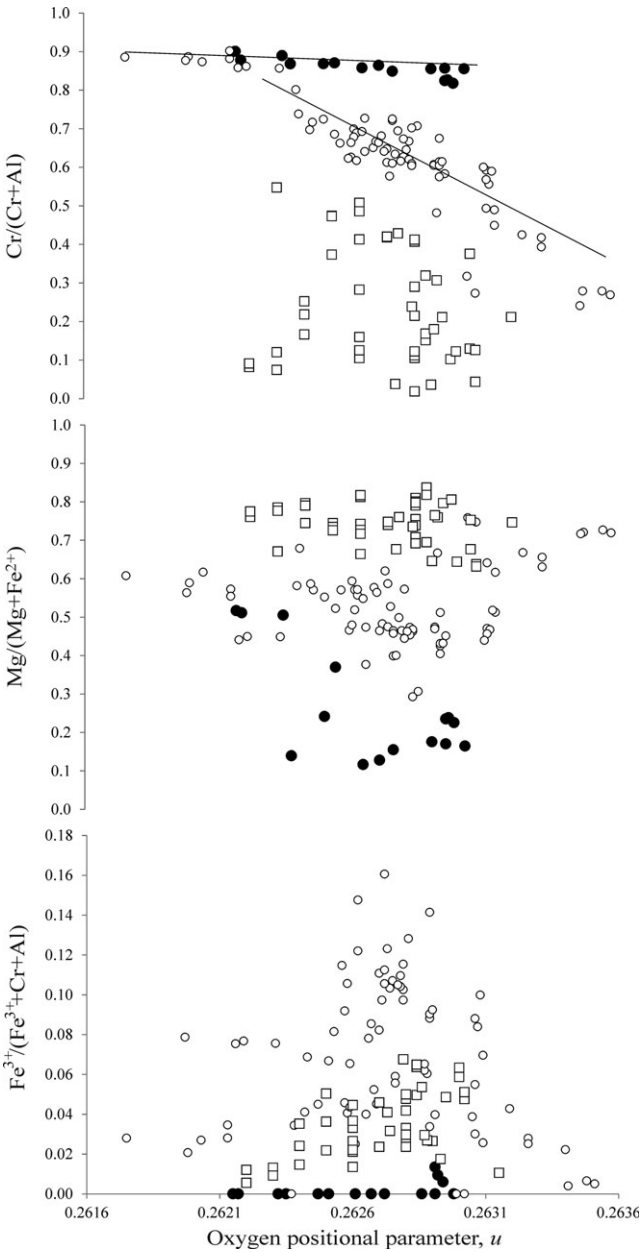

Fig. 5. Top to bottom Cr/(Cr + Al), Mg/(Mg + Fe^{2+}), and Fe^{3+}/(Fe^{3+} + Al + Cr) versus oxygen positional parameter, *u*. Black circle: extraterrestrial occurrences (this study and Lenaz et al. 2015); open circle: spinels from komatiites, kimberlites, and layered complexes (Lenaz et al. 2004a, 2007, 2009, 2012); open square: terrestrial mantle xenoliths (Della Giusta et al. 1986; Princivalle et al. 1989; Carraro 2003; Uchida et al. 2005). Lines in the top figure are a guide for the eye.

the sites is very limited due to the high amount of Cr and Fe, so maybe a coupled control by both Mg# and Cr# should be invoked. For spinels with limited Cr# variations (0.87–0.9) and large Mg# (0.1–0.5), there may be a control on the oxygen positional parameter given by Mg#, even if a clear trend is not present, but possibly, or more probably, some control is also exerted by the cooling history of the host rock.

To provide a better constrained model on the environmental conditions experienced by the two meteorites studied, we calculated the closure temperatures for the olivine-chromite pairs by using the Ballhaus et al. (1991) thermometer, by assuming a pressure set at 1 bar, that according to Benedix et al. (2005) is a reasonable assumption for the interior of bodies up to 100 km in radius. Previous studies on winonaites and silicate-bearing IAB irons showed a closure temperature for olivine-chromite pairs ranging from about 590° C to about 700° C with oxygen fugacities ranging 2.3–3.2 log units below the iron-wustite buffer by using the Sack and Ghiorso (1991) thermometer. Ganguly et al. (2013), however, noticed that for some H chondrites, there were differences between the temperatures calculated with the Sack and Ghiorso (1991) or the Ballhaus et al. (1991) thermometers with the last usually lower than the first. Moreover, they argued that there could be some problems with the Ol-Spl thermometer even if, especially the one by Ballhaus et al. (1991), is widely used, due to some possible resetting. We recalculated the temperatures and oxygen fugacities of the winonaites and silicate-bearing IAB by Benedix et al. (2005) and found that the temperatures are in the range 697–840° C (slightly higher than those calculated with the Sack and Ghiorso thermometer). Oxygen fugacities calculated by using the O'Neill (1987) oxybarometry are between −18.0 and −21.7. Our calculations show a temperature in the range 737–765° C (Ballhaus et al. [1991] thermometer) and a logfO_2 (O'Neill [1987] oxybarometer) in the range −19.8 to −20.5 for the NWA 725 (Fig. 6). The here studied winonaites and those studied by Benedix et al. (2005) fall more or less on the same line, slightly higher than the IW buffer.

Cr-spinels from NWA 725 differ from those of other winonaites mainly in term of Cr#, while the olivine-chromite pair thermometer registers similar closure temperature. It is interesting that both chemistry and structure of the spinels from NWA 725 resemble spinels from terrestrial komatiites, kimberlites, or spinels included in diamonds.

NWA 6077 shows temperatures between 846 and 884° C. For this meteorite, the logfO_2 is in the range −17.0 to −17.9 just above the iron-wustite buffer similarly to the brachinites studied by Shearer et al. (2010) and those reviewed in Keil (2014). Notably the majority of the

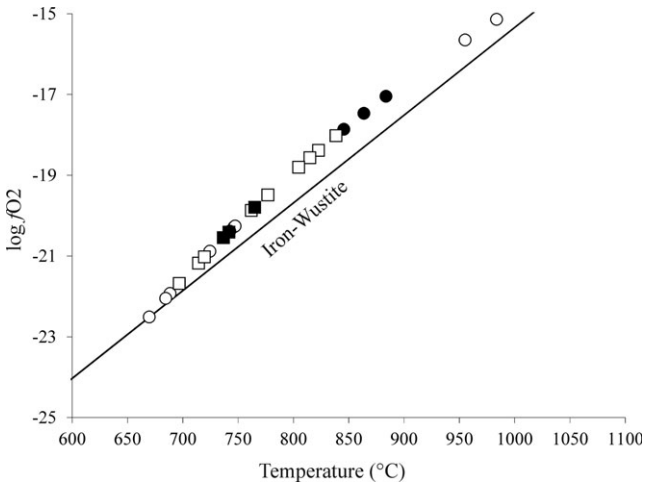

Fig. 6. Log fO_2 versus closure temperatures (°C). Black square: NWA 725 (this study); black circle: NWA 6077 (this study); open square: winonaites (Benedix et al. 2005); open circle: brachinites (Keil 2014).

spinels from brachinites fall in a range of temperatures that is close to that of chondrites, while NWA 6077 indicates higher temperatures comparable with those of spinels from pallasites, but lower than some spinels from brachinites reviewed in Keil (2014). In Fig. 7 are reported the closure temperatures versus olivine fayalite content of different chondrites and achondrites. It is possible to see how most of the winonaites and brachinites fall in the field representing the average Ol-Spl equilibration temperature of chondrites as seen in Sack and Ghiorso (1991). The here studied brachinites as well as some other brachinites, pallasites, and winonaites from literature show a higher equilibration temperature (Fig. 7).

CONCLUSIONS

Single-crystal X-ray diffraction and structural refinement show the differences between the studied spinels from brachinite-like and winonaite achondrites and spinels from chondrites previously analyzed (Lenaz et al. 2015).

Spinels from the NWA 725 winonaite present a cell edge in the range 8.3362 (1) to 8.3433 (4) Å and an oxygen positional parameter in the range 0.2622 (1) to 0.2623 (1). Estimated closure temperatures (olivine–chromite thermometer by Ballhaus et al. 1991) are between 737 and 765° C with a logfO_2 in the range −19.8 to −20.5 (oxybarometer by O'Neill 1987), i.e., just above the iron-wustite buffer. They differ from other winonaite spinels in having a lower Cr#, while showing similar olivine–chromite closure temperatures and oxygen fugacities.

Spinels from brachinite-like NWA 6077 present a cell edge in the range 8.3331 (2) to 8.3352 (1) Å and an oxygen positional parameter in the range 0.2629 (1) to

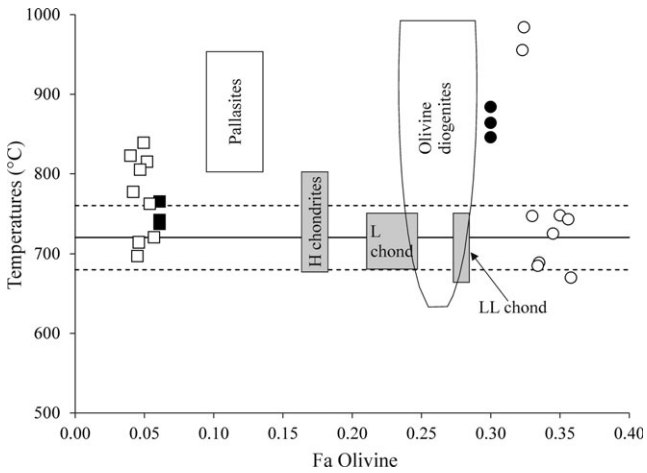

Fig. 7. Closure temperatures (°C) versus olivine fayalite content. Black square: NWA 725 (this study); black circle: NWA 6077 (this study); open square: winonaites (Benedix et al. 2005); open circle: brachinites (Keil 2014). Horizontal continuous and dashed lines indicate the respective mean and 1σ range of olivine-spinel Fe-Mg exchange temperatures calculated for ordinary chondrites from chromite and olivine data reported in Sack and Ghiorso (1991). Fields for pallasites, olivine diogenites, H, L, and LL chondrites after Sack and Ghiorso (1991).

0.2630 (1). Estimated closure temperatures are between 846 and 884° C with a $\log fO_2$ in the range −17.0 to −17.9, i.e., just above the iron-wustite buffer. They are similar to low-Al spinels from brachinites in Cr# and Mg#. The range of closure temperatures is very variable for brachinites.

The *u* values for terrestrial samples can give information about the cooling history of the samples, for the extraterrestrial samples it seems that the *u* values can give information about the cooling only for spinels where its value is lower than 0.2625. For higher values, it seems related only to the chemistry of the spinels.

Acknowledgments—The Italian C.N.R. financed the installation and maintenance of the microprobe laboratory in Padua. R. Carampin and L. Tauro are kindly acknowledged for technical support. This work was supported with an Advanced Grant from the European Research Council to BS, FRA2009 and PRIN 2010-11 to DL. G. Benedix is kindly acknowledged for her comments on a previous version of the manuscript. R. Downs, two anonymous reviewers, and the editorial handling of C. Goodrich are kindly acknowledged.

Editorial Handling—Dr. Cyrena Goodrich

REFERENCES

Andreozzi G. B. and Lucchesi S. 2002. Intersite distribution of Fe^{2+} and Mg in the spinel (sensu stricto)-hercynite series by single-crystal X-ray diffraction. *American Mineralogist* 87:1113–1120.

Ballhaus C., Berry R. F., and Green D. H. 1991. High pressure experimental calibration of the olivine-orthopyroxene-spinel oxygen geobarometer: Implications for the oxidation state of the upper mantle. *Contributions to Mineralogy and Petrology* 107:27–40.

Barnes S. J. and Roeder P. L. 2001. The range of spinel compositions in terrestrial mafic and ultramafic rocks. *Journal of Petrology* 42:2279–2302.

Basso R., Comin-Chiaramonti P., Della Giusta A., and Flora O. 1984. Crystal chemistry of four Mg-Fe-Al-Cr spinels from the Balmuccia peridotite (Western Italian Alps). *Neues Jahrbuch für Mineralogie Abhandlungen* 150:1–10.

Benedix G. K., McCoy T. J., Keil K., Bogard D. D., and Garrison D. H. 1998. A petrologic and isotopic study of winonaites: Evidence for early partial melting, brecciation and metamorphism. *Geochimica et Cosmochimica Acta* 62:2535–2553.

Benedix G. K., Lauretta D. S., and McCoy T. J. 2005. Thermodynamic constraints on the formation conditions of winonaites and silicate-bearing IAB irons. *Geochimica et Cosmochimica Acta* 69:5123–5131.

Bosi F., Andreozzi G. B., Ferrini V., and Lucchesi S. 2004. Behavior of cation vacancy in kenotetrahedral Cr-spinels from Albanian eastern belt ophiolites. *American Mineralogist* 89:1367–1373.

Buchanan P. E. and Reid A. M. 1996. Petrology of the polymict eucrite Petersburg. *Geochimica et Cosmochimica Acta* 60:135–146.

Bunch T. E. and Keil K. 1971. Chromite and ilmenite in non-chondritic meteorites. *American Mineralogist* 56:146–157.

Bunch T. E., Keil K., and Snetsinger K. G. 1967. Chromite composition in relation to chemistry and texture of ordinary chondrites. *Geochimica et Cosmochimica Acta* 31:1569–1582.

Bunch T. E., Keil K., and Olsen E. 1970. Mineralogy and petrology of silicate inclusions in iron meteorites. *Contributions to Mineralogy and Petrology* 25:297–340.

Carbonin S., Russo U., and Della Giusta A. 1996. Cation distribution in some natural spinels from X-ray diffraction and Mössbauer spectroscopy. *Mineralogical Magazine* 60:355–368.

Carbonin S., Menegazzo G., Lenaz D., and Princivalle F. 1999. Crystal chemistry of two detrital Cr-spinels with unusual low values of oxygen positional parameter: Oxidation mechanism and possible clues to their origin. *Neues Jahrbuch für Mineralogie Monatshefte* 359–371.

Carraro A. 2003. Crystal chemistry of Cr-spinels from a suite of spinel peridotite mantle xenoliths from the Predazzo Area (Dolomites, Northern Italy). *European Journal of Mineralogy* 15:681–688.

Choi B.-G., Oyuyang X., and Wasson J. T. 1995. Classification and origin of IAB and IIICD iron meteorites. *Geochimica et Cosmochimica Acta* 59:593–612.

Christophe Michel-Levy M., Bourot-Denise M., Palme H., Spettel B., and Wänke H. 1987. L'eucrite de Bouvante: Chimie, pétrologie et minéralogie. *Bullettin de Minéralogie* 110:449–458.

Day J. M. D., Walker R. J., Ash R. D., Liu Y., Rumble D. III, Irving A. J., Goodrich C. A., Tait K., McDonough W. F., and Taylor L. A. 2012. Origin of felsic achondrites Graves Nunataks 06128 and 06129, and ultramafic brachinites and brachinite-like achondrites by partial

melting of volatile-rich primitive parent bodies. *Geochimica et Cosmochimica Acta* 81:94–128.

Della Giusta A., Princivalle F., and Carbonin S. 1986. Crystal chemistry of a suite of natural Cr-bearing spinels with $0.15 < Cr < 1.07$. *Neues Jahrbuch für Mineralogie Abhlandungen* 155:319–330.

Della Giusta A., Carbonin S., and Ottonello G. 1996. Temperature-dependant disorder in a natural Mg-Al-Fe^{2+}-Fe^{3+}-spinel. *Mineralogical Magazine* 60:603–616.

Derbyshire E. J., O'Driscoll B., Lenaz D., Gertisser R., and Kronz A. 2013. Compositional heterogeneity in chromitite seams from the Shetland Ophiolite Complex (Scotland): Implications for chromitite petrogenesis and late-stage alteration in the upper mantle portion of a supra-subduction zone ophiolite. *Lithos* 162–163:279–300.

Dick H. J. B. and Bullen T. 1984. Chromian spinel as a petrogenetic indicator in abyssal and alpine-type peridotites and spatially associated lavas. *Contributions to Mineralogy and Petrology* 86:54–76.

Floss C., Crozaz G., Jolliff B., Benedix G., and Colton S. 2008. Evolution of the winonaite parent body: Clues from silicate mineral trace element distributions. *Meteoritics & Planetary Science* 43:657–674.

Ganguly J., Tirone M., Chakraborty S., and Domanik K. 2013. H-chondrite parent asteroid: A multistage cooling, fragmentation and re-accretion history constrained by thermometric studies, diffusion kinetics modeling and geochronological data. *Geochimica et Cosmochimica Acta* 105:206–220.

Garvie L. A. J. 2012. The Meteoritical Bulletin 99. *Meteoritics & Planetary Science* 47:E1–E52.

Goodrich C. A., Van Orman J. A., and Wilson L. 2007. Fractional melting and smelting of the ureilite parent body. *Geochimica et Cosmochimica Acta* 71:2876–2895.

Goodrich C. A., Harlow G. E., Van Orman J. A., Sutton S. R., Jercinovic M. J., and Mikouchi T. 2014. Petrology of chromite in ureilites: Deconvolution of primary oxidation states and secondary reduction processes. *Geochimica et Cosmochimica Acta* 135:126–169.

Greenwood R. C., Franchi I. A., Gibson J. M., and Benedix G. K. 2012. Oxygen isotope variation in primitive achondrites: The influence of primordial, asteroidal and terrestrial processes. *Geochimica et Cosmochimica Acta* 94:146–163.

Grossman J. N. and Zipfel J. 2001. The Meteoritical Bulletin 85. *Meteoritics & Planetary Science* 36:A293–A322.

Irvine T. N. 1967. Chromian spinel as a petrogenetic indicator. Part 2. Petrologic applications. *Canadian Journal of Earth Science* 4:71–103.

Kamenetsky V. S., Crawford A. J., and Meffre S. 2001. Factors controlling chemistry of magmatic spinel: An empirical study of associated olivine, Cr-spinel and melt inclusions from primitive rocks. *Journal of Petrology* 42:655–671.

Keil K. 2014. Brachinite meteorites: Partial melt residues from an FeO-rich asteroid. *Chemie der Erde* 74:311–329.

Lavina B., Salviulo G., and Della Giusta A. 2002. Cation distribution and structure modeling of spinel solid solutions. *Physics and Chemistry of Minerals* 29:10–18.

Lenaz D. and Skogby H. 2013. Structural changes in the $FeAl_2O_4$-$FeCr_2O_4$ solid solution series and their consequences on natural Cr-bearing spinels. *Physics and Chemistry of Minerals* 40:587–595.

Lenaz D., Kamenetsky V., Crawford A. J., and Princivalle F. 2000. Melt inclusions in detrital spinel from SE Alps (Italy-Slovenia): A new approach to provenance studies of sedimentary basins. *Contributions to Mineralogy and Petrology* 139:748–758.

Lenaz D., Carbonin S., Gregoric M., and Princivalle F. 2002. Crystal chemistry and oxidation state of one euhedral Cr-spinel crystal enclosed in a bauxite layer (Trieste Karst: NE Italy): Some considerations on its depositional history and provenance. *Neues Jahrbuch für Mineralogie Monatshefte* 193–206.

Lenaz D., Andreozzi G. B., Mitra S., Bidyananda M., and Princivalle F. 2004a. Crystal chemical and ^{57}Fe Mössbauer study of chromite from the Nuggihalli schist belt (India). *Mineralogy and Petrology* 80:45–57.

Lenaz D., Skogby H., Princivalle F., and Hålenius U. 2004b. Structural changes and valence states in the $MgCr_2O_4$-$FeCr_2O_4$ solid solution series. *Physics and Chemistry of Minerals* 31:633–642.

Lenaz D., Skogby H., Princivalle F., and Hålenius U. 2006. The $MgCr_2O_4$-$MgFe_2O_4$ solid solution series: Effects of octahedrally coordinated Fe^{3+} on T-O bond lengths. *Physics and Chemistry of Minerals* 33:465–474.

Lenaz D., Braidotti R., Princivalle F., Garuti G., and Zaccarini F. 2007. Crystal chemistry and structural refinement of chromites from different chromitite layers and xenoliths of the Bushveld Complex. *European Journal of Mineralogy* 19:599–609.

Lenaz D., Logvinova A. M., Princivalle F., and Sobolev N. V. 2009. Structural parameters of chromite included in diamonds and kimberlites from Siberia: A new tool for discriminating ultramafic source. *American Mineralogist* 94:1067–1070.

Lenaz D., De Min A., Garuti G., Zaccarini F., and Princivalle F. 2010. Crystal chemistry of Cr-spinels from the lherzolite mantle peridotite of Ronda (Spain). *American Mineralogist* 95:1323–1328.

Lenaz D., O'Driscoll B., and Princivalle F. 2011. Petrogenesis of the anorthosite-chromitite association: Crystal-chemical and petrological insights from the Rum Layered Suite, NW Scotland. *Contributions to Mineralogy and Petrology* 162:1201–1213.

Lenaz D., Garuti G., Zaccarini F., Cooper R. W., and Princivalle F. 2012. The Stillwater Complex: The response of chromite crystal chemistry to magma injection. *Geologica Acta* 10:33–41.

Lenaz D., Skogby H., Logvinova A. M., Sobolev N. V., and Princivalle F. 2013. A micro-Mössbauer study of chromites included in diamond and other mantle-related rocks. *Physics and Chemistry of Minerals* 40:671–679.

Lenaz D., Adetunji J., and Rollinson H. 2014a. Determination of $Fe^{3+}/\Sigma Fe$ ratios in chrome spinels using a combined Mössbauer and single-crystal X-ray approach: Application to chromitites from the mantle section of the Oman ophiolite. *Contributions to Mineralogy and Petrology* 167:958.

Lenaz D., Andreozzi G. B., Bidyananda M., and Princivalle F. 2014b. Oxidation degree of chromite from Indian ophiolites: A crystal chemical and ^{57}Fe Mössbauer study. *Periodico di Mineralogia* 83:241–255.

Lenaz D., Youbi N., De Min A., Boumehdi M. A., and Ben Abbou M. 2014c. Low intra-crystalline closure temperatures of Cr-bearing spinels from the mantle xenoliths of the Middle Atlas Neogene-Quaternary

Volcanic Field (Morocco): A mineralogical evidence of a cooler mantle beneath the West African Craton. *American Mineralogist* 99:267–275.

Lenaz D., Princivalle F., and Schmitz B. 2015. First crystal-structure determination of chromites from an acapulcoite and ordinary chondrites. *Mineralogical Magazine* 79:755–765.

Lenaz D., Velicogna M., Hålenius U., and O'Driscoll B. 2016. Structural parameters of Cr-bearing spinels and pleonaste from the Cuillin Igneous Complex (Isle of Skye, Scotland): Implications for metamorphic and cooling history. *Mineralogical Magazine* 80:749–764.

Lenaz D., Musco M. E., Petrelli M., Caldeira R., De Min A., Marzoli A., Mata J., Perugini D., Princivalle F., Boumehdi M. A., Bensaid I. A. A., and Youbi N. 2017. Restitic or not? Insights from trace element content and crystal—Structure of spinels in African mantle xenoliths. *Lithos* 287–281:464–476. doi: 10.1016/j.lithos.2017.02.012.

Lindsley D. H. 1976. The crystal chemistry and structure of oxide minerals as exemplified by the Fe-Ti oxides. In *Oxide minerals*, edited by Rumble D. III. Chelsea, Michigan: Mineralogical Society of America. pp. 1–60.

Lovering J. F. 1975. The Moama eucrite—A pyroxene-plagioclase adcumulate. *Meteoritics* 10:101–114.

McCoy T. J., Keil K., Clayton R. N., and Mayeda T. K. 1993. Classification parameters for acapulcoites and lodranites: The cases of FRO 90011, EET 84302 and ALH A81187/84190 (abstract). 44th Lunar and Planetary Science Conference. pp. 945–946.

McCoy T. J., Clayton R. N., Mayeda T. K., Bogard D. D., Garrison D. H., and Wieler R. 1997. A petrologic and isotopic study of lodranites: Evidence for early formation as partial melt residues from heterogeneous precursors. *Geochimica et Cosmochimica Acta* 61:639–650.

McCoy T., Mittlefehldt D. W., and Wilson L. 2006. Asteroid differentiation. In *Meteorites and the early solar system II*, edited by Lauretta D. S. and McSween H. Y. Tucson, Arizona: University of Arizona Press. pp. 733–745.

Mittlefehldt D. W. 1994. The genesis of diogenites and HED parent body petrogenesis. *Geochimica et Cosmochimica Acta* 58:1537–1552.

Mittlefehldt D. W. and Lindstrom M. M. 1993. Geochemistry and petrology of a suite of ten Yamato HED meteorites. *Proceedings NIPR Symposium Antarctic Meteorites* 6:268–292.

Mittlefehldt D. W., Lindstrom M. M., Bogard D. D., Garrison D. H., and Field S. W. 1996. Acapulco- and Lodran-like achondrites: Petrology, geochemistry, chronology and origin. *Geochimica et Cosmochimica Acta* 60:867–882.

Mittlefehldt D. W., McCoy T. J., Goodrich C. A., and Kracher A. 1998. Non-chondritic meteorites from asteroidal bodies. In *Planetary materials*, edited by Papike J. J. *Reviews in Mineralogy* 36:195–232.

Mittlefehldt D. W., Bogard D. D., Berkley J. L., and Garrison D. H. 2003. Brachinites: Igneous rocks from a differentiated asteroid. *Meteoritics & Planetary Science* 38:1601–1625.

Nakatsuka A., Ueno H., Nakayama N., Mizota T., and Maekawa H. 2004. Single-crystal X-ray diffraction study of cation distributiom in $MgAl_2O_4$-$MgFe_2O_4$ spinel solid solution. *Physics and Chemistry of Minerals* 31:278–287.

Nédli Z., Princivalle F., Lenaz D., and Tóth T. M. 2008. Crystal chemistry of clinopyroxene and spinel from mantle xenoliths hosted in Late Mesozoic lamprophyres (Villány Mts, S Hungary). *Neues Jahrbuch für Mineralogie Abhandlungen* 185:1–10.

North A. C. T., Phillips D. C., and Scott-Mattews F. 1968. A semi-empirical method of absorption correction. *Acta Crystallographica* A24:351–352.

O'Neill H. St. C. 1987. The quartz-fayalite-iron and quartz-fayalite-magnetite equilibria and the free energies of formation of fayalite (Fe_2SiO_4) and magnetite (Fe_3O_4). *American Mineralogist* 72:67–75.

O'Neill H. St. C. and Navrotsky A. 1984. Cation distributions and thermodynamic properties of binary spinel solid solutions. *American Mineralogist* 69:733–753.

Parisi F., Lenaz D., Princivalle F., and Sciascia L. 2014. Ordering kinetics in synthetic $Mg(Al, Fe^{3+})_2O_4$ spinels: First quantitative elucidation of the whole Al-Mg-Fe partitioning, rate constants, activation energies and implication for geothermometry. *American Mineralogist* 99:2203–2210.

Perinelli C., Bosi F., Andreozzi G. B., Conte A. M., and Armienti P. 2014. Geothermometric study of Cr-spinels of peridotite mantle xenoliths from Northern Victoria Land (Antarctica). *American Mineralogist* 99:839–846.

Prince E. 2004. International tables for x-ray crystallography. In *Volume C: Mathematical, physical and chemical tables*. 3rd ed. Dordrecht, the Netherlands: Springer. p. 1000.

Princivalle F., Della Giusta A., and Carbonin S. 1989. Comparative crystal chemistry of spinels from some suites of ultramafic rocks. *Mineralogy and Petrology* 40: 117–126.

Princivalle F., De Min A., Lenaz D., Scarbolo M., and Zanetti A. 2014. Ultramafic xenoliths from Damaping (Hannuoba region, NE-China): Petrogenetic implications from crystal chemistry of pyroxenes, olivine and Cr-spinel and trace element content of clinopyroxene. *Lithos* 188:3–14.

Rollinson H., Adetunji J., Lenaz D., and Szilas K. 2017. Archaean chromitites show constant $Fe^{3+}/\Sigma Fe$ in Earth's asthenospheric mantle since 3.8 Ga. *Lithos* 282–283:316–325.

Sack R. O. and Ghiorso M. S. 1991. Chromite as a Petrogenetic indicator. In *Oxide minerals: Petrologic and magnetic significance*, edited by Lindsley D. H. *Reviews in Mineralogy* 25:323–353.

Sanborn M. E., Yin Q.- Z., Schmitz B., and Amelin Y. 2016. Northwest Africa 5400/6077: Deciphering the origin of the mysterious achondrite with a new look at the isotopic composition (abstract #2309). 47th Lunar and Planetary Science Conference. CD-ROM.

Schreiber H. D. and Haskin L. A. 1976. Chromium in basalts: Experimental determination of redox states and partitioning among synthetic silicate phases. Proceedings, 7th Lunar Science Conference. pp. 1221–1259.

Seifert S. and Ringwood A. E. 1988. The lunar geochemistry of chromium and vanadium. *Earth, Moon, and Planets* 40:45–70.

Shearer C. K., Burger P. V., Neal C., Sharp Z., Spivak-Birndorf L., Borg L., Fernandes V. A., Papike J. J., Karner J., Wadhwa M., Gaffney A., Shafer J., Geissman J., Atidorei N.-V., Herd C., Weiss B. P., King P. L., Crowther S. A., and Gilmour J. D. 2010. Non-basaltic asteroidal magmatism during the earliest stages of solar system evolution: A view from Antarctic achondrites

Graves Nunataks 06128 and 06129. *Geochimica et Cosmochimica Acta* 74:1172–1199.

Sheldrick G. M. 2008. A short history of SHELX. *Acta Crystallographica* A64:112–122.

Sutton S. R., Jones K. W., Gordon B., Rivers M. L., Bajt S., and Smith J. V. 1993. Reduced chromium in olivine grains from lunar basalt 15555: X-ray absorption near edge structure (XANES). *Geochimica et Cosmochimica Acta* 57:461–468.

Takeda H., Bogard D. D., Mittlefehldt D. W., and Garrison D. H. 2000. Mineralogy, petrology, chemistry and ^{39}Ar-^{40}Ar and exposure ages of the Caddo County IAB iron: Evidence for early partial melt segregation of a gabbro area rich in plagioclase-diopside. *Geochimica et Cosmochimica Acta* 64:1311–1327.

Tokonami M. 1965. Atomic scattering factor for O^{-2}. *Acta Crystallographica* 19:486.

Touboul M., Kleine T., Bourdon B., van Orman J. A., Maden C., and Zipfel J. 2009. Hf–W thermochronometry: II. Accretion and thermal history of the acapulcoite–lodranite parent body. *Earth and Planetary Science Letters* 284:168–178.

Uchida H., Lavina B., Downs R. T., and Chesley J. 2005. Single-crystal X-ray diffraction of spinels from the San Carlos volcanic field, Arizona: Spinel as a geothermometer. *American Mineralogist* 90:1900–1908.

Warren P. H., Ulff-Møller F., Huber H., and Kallemeyn G. W. 2006. Siderophile geochemistry of ureilites: A record of early stages of planetesimal core formation. *Geochimica et Cosmochimica Acta* 70:2104–2126.

Weisberg M. K., McCoy T. J., and Krot A. N. 2006. Systematics and evaluation of meteorite classification. In *Meteorites and the early solar system II*, edited by Lauretta D. S. and McSween H. Y. Jr. Tucson, Arizona: University of Arizona Press. pp. 19–52.

Yamaguchi A., Takeda H., Bogard D. D., and Garrison D. 1994. Textural variation and impact history of the Millillillie eucrite. *Meteoritics* 29:237–245.